Biochemical Pharmacology, Vol. 54, pp. 1181–1193, 1997.

ELSEVIER

ISSN 0006-2952/97/$17.00 + 0.00
PII S0006-2952(97)00321-3

Effects on DNA Integrity and Apoptosis Induction by a Novel Antitumor Sesquiterpene Drug, 6-Hydroxymethylacylfulvene (HMAF, MGI 114)

Jan M. Woynarowski,† Cheryl Napier,* Steven K. Koester,*¶ Shih-Fong Chen,* Dean Troyer,‡ William Chapman* and John R. MacDonald§*

*Cancer Therapy and Research Center and ‡UT Health Science Center, San Antonio, TX; and §MGI PHARMA, INC., Minnetonka, MN

ABSTRACT. 6-Hydroxymethylacylfulvene (HMAF, MGI 114) is a new alkylating antitumor sesquiterpenoid with promising and often curative antitumor activity *in vivo*. This study examined the ability of the drug to damage cellular DNA, induce apoptosis, and affect the cell cycle of CEM human leukemia cells. No bifunctional lesions, interstrand DNA cross-links or DNA–protein cross-links were seen (by alkaline sedimentation and K^+/SDS precipitation, respectively) when using up to 50 μM HMAF. The drug possibly formed some monoadducts, as DNA from drug-treated cells impeded primer extension by *Taq* polymerase, although only partial inhibition was seen even at 200 μM HMAF. HMAF also induced secondary lesions in cellular DNA, single-strand breaks that were detectable (by nucleoid sedimentation and alkaline sucrose gradient analysis) after a 4-hr treatment at HMAF levels as low as 2 μM, comparable to the growth inhibition IC_{50} value (1.7 μM). A post-treatment incubation of cells in drug-free medium generated substantial amounts of DNA double-stranded fragments of several kbp, suggesting apoptotic fragmentation (>30% of total DNA following treatment with 20 μM HMAF and a 17-hr post-treatment incubation). Chromatin condensation (by ultrastructural analysis) and induction of sub-G_1 particles and apoptotic strand breakage (by multiparametric flow cytometry) confirmed induction of apoptosis by HMAF. HMAF preferentially inhibited DNA synthesis ($IC_{50} \approx 2$ μM), which is consistent with an S phase block, observed by cell cycle analysis. The pattern of apoptotic DNA fragmentation, inhibition of DNA synthesis, and blockage in the S phase suggests that these events play a role in the antiproliferative activity of HMAF. BIOCHEM PHARMACOL **54**;11:1181–1193, 1997. © 1997 Elsevier Science Inc.

KEY WORDS. 6-hydroxymethylacylfulvene; apoptosis; DNA fragmentation; S phase block; cytotoxic activity

Illudins are cytotoxic sesquiterpenoids originally isolated from the fungi *Omphalotus illudens* and *Lampteromyces japonicus* [1–3]. While the lead natural compound, Illudin S (Fig. 1), showed preferential cytotoxicity against certain tumor cells *in vitro*, the agent and its analogs had only marginal antitumor activity *in vivo* [1, 2, 4, 5]. Systematic structure–activity relationship studies have led recently to the development of illudin analogs of the acylfulvene class with improved pharmacological properties [6]. One of these analogs, HMAF‖ (also called MGI 114) (Fig. 1) [7, 8], has demonstrated promising *in vivo* activity against several experimental tumor systems. Curative antitumor activity was found against human breast MX-1 tumor xenograft, MV522 human lung adenocarcinoma, and HT-29 colon carcinoma [9, 10].

Studies by other researchers have suggested that related illudins (Illudins S and M) may act as alkylating agents, possibly forming covalent adducts with DNA [1, 11, 12]. However, no published reports assessed the effects of HMAF on cellular DNA. Also, despite the very promising *in vivo* activities, very little is known about cellular effects that might contribute to the mechanism of cytotoxicity of HMAF and related drugs.

Our study examined the effects of HMAF on cellular DNA in relation to drug inhibition of cell growth and cell cycle progression. The results show that, while HMAF treatment affects the integrity of cellular DNA, these lesions are primarily indirect and reflect drug-induced apoptosis.

MATERIALS AND METHODS

Cells and Growth Conditions

Human CEM leukemia cells (provided by Dr. William T. Beck, St. Jude Children's Hospital, Memphis, TN) were

† Corresponding author: Jan M. Woynarowski, Ph.D., Head, Molecular Pharmacology, Cancer Therapy and Research Center, Institute for Drug Development, 14960 Omicron Dr., San Antonio, TX 78245-3217. Telephone (210) 677-3832; FAX (210) 677-0058; e-mail: jan@jerry.iddw.saci.org

‖*Abbreviations:* DPC, DNA–protein cross-links; EC_{50}, drug concentration inhibiting cell growth (MTT assay) by 50%; HMAF (MGI 114), 6-hydroxymethylacylfulvene; IC_{50}, drug concentration inhibiting the macromolecule precursor incorporation by 50%; MTT, 3-(4,5-dimethylthiazol-2-yl)-2,5-diphenyltetrazolium bromide; PCA, perchloric acid; PCR, polymerase chain reaction; PI, propidium iodide; PMSF, phenylmethylsulfonyl fluoride; QPCR, quantitative PCR; TdT, terminal deoxynucleotidyl transferase.

¶ Present address: Coulter Technology Center, Miami, FL.

Received 15 April 1997; accepted 2 June 1997.

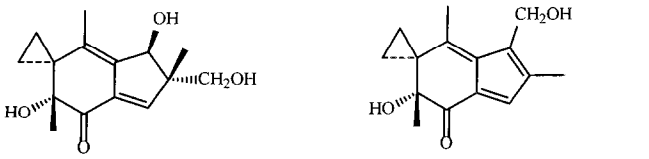

ILLUDIN S 6-HYDROXYMETHYLACYLFULVENE HMAF

FIG. 1. Structures of Illudin S and HMAF.

grown at 37° in a humidified incubator (with 5% CO_2) in Joklik's medium containing 10% fetal bovine serum. Except where noted otherwise, cell cultures were established at 2×10^5 cells/mL for experiments with HMAF.

Cytotoxic Activity

Growth inhibitory activity was assayed, as described previously [13], using the standard MTT assay. Exponentially growing cells in a 96-well microtiter plate were incubated with the drug for 3–4 doubling times (3–4 days for CEM cells) and subjected to colorimetric reaction with MTT. The results are expressed as EC_{50} values.

PCR Stop Assay

CEM cells were prelabeled by overnight incubation in medium containing 0.05 to 0.1 μCi/mL [^{14}C]thymidine. Then the cells were harvested and resuspended at 5×10^5 cells/mL in fresh medium for an additional hour at 37°, which was followed by a 4-hr incubation with various concentrations of HMAF. Following drug treatment, cells were washed by centrifugation with PBS, and their DNA was extracted and purified using the PureGene kit (Gentra Systems, Minneapolis, MN) according to the manufacturer's protocol. The concentrations of purified DNA were expressed as "cell equivalents" based on total ^{14}C radioactivity. A semi-quantitative PCR-stop assay was carried out using a primer system for a 536 bp segment of the β-globin gene and cycling conditions described by others [14]. PCR reactions (20 μL) usually were carried out in triplicate at two to three different levels of template DNA (1000–5000 cell equivalents per reaction). Following electrophoresis in 1% agarose and autoradiography, signal intensities were quantitated in a Molecular Dynamics densitometer. The results are normalized to the signal intensity in control samples and averaged for replicates and the different levels of template DNA.

DPC

CEM cells were prelabeled with [^{14}C]thymidine as outlined for the PCR-stop assay. Aliquots of cell suspension were treated with HMAF, as indicated, and next were subjected to K^+/SDS precipitation to determine the percentage of DNA covalently bound to proteins [15].

Interstrand Cross-links and Single-Strand Breaks

The previously described procedure for sedimentation analysis of cellular DNA [16] was used with some modifications. Cells were prelabeled with [^{14}C]thymidine as described for the PCR-stop assay. HMAF was added and cells were incubated as indicated in the legend to Fig. 2. Treated cells were collected by centrifugation, washed twice with PBS, and resuspended in 670 μL of hypotonic buffer (50 mM Tris–HCl, pH 7.5, 10 mM EDTA, 0.2% Triton X-100). Approximately 1.1×10^5 cells (in 150 μL) were loaded onto pre-formed alkaline sucrose gradients composed of 0.5 mL of 60% sucrose cushion, 10 mL of 5–20% sucrose, and 0.2 mL lysing layer (1% sarkosyl, 2.5% sucrose). All the solutions were in gradient buffer (0.7 M NaCl, 0.3 M NaOH, 0.01 M EDTA). Following sample application, an additional volume (200 μL) of lysing solution was laid on the top, and lysis was allowed to proceed for 20 hr (for DNA cross-links) or 14 hr (for DNA breaks). Following lysis, samples were centrifuged for 20 hr at 9,500 rpm (for DNA cross-links) or 10 hr at 17,500 rpm (for DNA breaks) in an SW41 rotor (Beckman Instruments Inc., Fullerton, CA). Gradients were fractionated from the top into 24 fractions, neutralized with 1 mL of 0.15 M HCl per fraction, and counted in a liquid scintillation counter. Sedimentation profiles were determined by calculating the percentage of recovered radioactivity in each sample. To determine total [^{14}C]thymidine incorporation, a 150-μL aliquot of each cell suspension was hydrolyzed by incubation in 0.5 M PCA for 2 hr at 65°. Recovery of radioactivity was typically greater than 85%. Molecular weights of DNA in gradient fractions were calculated as described previously [16].

Nucleoid Sedimentation

Cells were prelabeled with [^{14}C]thymidine as described for the DPC assay and treated with HMAF as indicated. Nucleoids from HMAF-treated cells were prepared and analyzed as described previously [17]. Briefly, cells were washed with PBS and suspended in 800 μL PBS. Aliquots of cell suspensions (200 μL) were loaded onto 10 mL preformed neutral sucrose gradients (5–30% sucrose in 1.9 M NaCl, 50 mM Tris, 20 mM EDTA, pH 8.0) with 0.4 mL lysing layers (0.7% Triton X-100 in 1.9 M NaCl, 50 mM Tris, 20 mM EDTA, pH 8.0). Samples were allowed to lyse for 45 min on the gradient and were then centrifuged for 90 min at 17,000 rpm in a Beckman SW41 rotor. Following centrifugation, gradients were fractionated from the top into 24 fractions. Each fraction was diluted with 1 mL water, mixed with scintillation fluid, and counted in a liquid scintillation counter. Sedimentation profiles were determined by calculating the percentage of recovered radioactivity in each fraction. Total [^{14}C]thymidine incorporation was determined as described for the alkaline sucrose gradients. Recovery of radioactivity was typically greater than 85%.

Release of DNA Fragments

This assay is an adaptation of a common procedure for the generation of short, presumably apoptotic, double-stranded DNA fragments [18]. Cellular DNA was prelabeled with [^{14}C]thymidine as described for DNA–protein cross-links. The cells (2×10^5 cells/mL) were treated with HMAF or doxorubicin (a positive control) [18, 19] for 4 hr, centrifuged, and incubated in a fresh drug-free medium for an additional 17 hr. Control cultures were incubated without drug for 21 hr. Cells were washed with PBS, suspended in 300 μL hypotonic buffer (10 mM Tris, pH 7.5, 10 mM EDTA, 0.1 mM PMSF, 0.2% Triton X-100), and incubated on ice for 1 hr. Permeabilized cells were centrifuged for 5 min at 4° at 14,000 *g* in a microcentrifuge. The supernatants (S1) were collected, and the pellets (P1) were suspended in 2 mM EDTA and incubated for an additional 2 hr on ice. Samples were centrifuged as before, and the supernatants (S2) were collected. The remaining pellets (P2) containing unfragmented DNA were hydrolyzed by incubating with 300 μL of 0.5 M PCA at 75° for 30 min. Both the supernatants and the hydrolyzed pellets were counted on a microplate liquid scintillation counter (Top Count, Packard Instrument Co., Meriden, CT). The results are expressed as the percentage of the total DNA released in the combined supernatants (S1 + S2):

$$\text{Released fragments [\%]} = \frac{\text{cpm S1} + \text{cpm S2}}{\text{cpm S1} + \text{cpm S2} + \text{cpm P2}}$$

Occasionally, culture medium and PBS washes were also counted to ascertain that no significant amounts of labeled DNA were leaking from the cells before the permeabilization. To measure the size of the released fragments (see Fig. 5B), the combined S1 and S2 supernatants were concentrated by spin dialysis and electrophoresed in 0.8% agarose followed by autoradiography of the dried gel.

In additional experiments, DNA from unlabeled HMAF-treated cells was analyzed for the presence of nucleosome-size fragments [20] by electrophoresis in 1% agarose. In these determinations, the equivalent of up to 20×10^6 cells per lane was used.

Drug Treatment for Cell Cycle Analysis, TdT Assay, and Electron Microscopy

CEM cells were seeded at 1.5×10^5 cells/mL for the 72-hr experiment or at 2×10^5 for the 17-hr experiment. HMAF was added at concentrations of 1.7, 3.5, and 8.5 μM, which corresponded to 1x, 2x, and 5x the EC_{50} for HMAF growth inhibition of CEM cells. At the indicated times, cells were counted in a hemocytometer to determine total cell concentration and cell viability (by trypan blue exclusion). Aliquots corresponding to 1×10^6 cells were processed as described below.

Cell Cycle Distribution and TdT Assay for Identification of Apoptotic Cells

Apoptotic lesions in cellular DNA were monitored based on biotin-tagging of 3′-OH ends resulting from apoptotic fragmentation with TdT followed by immunofluorescent detection of the biotin label [21, 22]. Briefly, HMAF-treated and control CEM cells were fixed with 1% EM grade paraformaldehyde (Electron Microscopy Sciences, Fort Washington, PA) in PBS at room temperature for 15 min. Fixed cells were washed with PBS, resuspended in cold PBS, and mixed with cold (−20°) absolute ethanol (70% final concentration) and stored at 4° in the dark. Aliquots of 1.0×10^6 cells were washed twice with cold (4°) PBS by centrifuging for 6 min at $200 \times g$. Cell pellets were resuspended in 50 μL of TdT reaction mixture (final concentrations: 0.2 M potassium cacodylate; 25 mM Tris–HCl, pH 6.6; 0.25 mg/mL bovine serum albumin; 2.5 mM $CoCl_2$; 12.5 U TdT; 10 μM biotin-dUTP, all reagents from the Boehringer Mannheim Kit No. 220-582) and incubated for 60 min at 37°. For each test sample, a parallel reaction without the enzyme was run to provide background staining. After washing with PBS, cells were incubated with fluorescein-labeled avidin (FITC-avidin 2.5 μg/mL, VECTOR Laboratories, Inc., Burlingame, CA) in 100 μL of reaction buffer (60 mM sodium citrate, 0.6 M NaCl, pH 7.5, with 0.1% Triton X-100) for 60 min at room temperature in the dark. Finally, cells were washed with PBS, and counterstained in 1.0 mL of 5.0 μg/mL PI in PBS. Flow cytometric measurements were collected on a Coulter EPICS ELITE flow cytometer using a 488 nm excitation from the argon ion laser. The FITC and PI signals were collected as a measure of 3′-OH ends and DNA content, respectively. FITC and PI fluorescence emissions were split using a 550-nm dichroic filter, with the FITC emission collected through a 525/530 nm filter and the PI emission collected through a 675 nm long pass filter. Additionally, forward- and side-light-scattering data were collected. Histograms (based on 30,000 events) were analyzed for cell cycle compartments and apoptotic cells using MultiCycle Advanced Version software (Phoenix Flow Systems). The flow cytometry experiments shown in Fig. 5 analyzed only DNA content based on PI fluorescence. In that case, the fixation step with paraformaldehyde was omitted, and the harvested cells were fixed in 70% ethanol and stained with PI before collecting one-parameter flow cytometry measurements (based on 50,000 events).

Electron Microscopy

Harvested cells were fixed with 2.5% glutaraldehyde (EM grade) in PBS for a minimum of 1 hr, washed with PBS, post-fixed in 1% osmium tetroxide for 1 hr, and embedded for preparing semi-thin (1 μm) and thin sections. Semi-thin sections were evaluated by light microscopy for the appearance of chromatin condensation. Thin sections were stained with saturated uranyl acetate and lead citrate and

TABLE 1. QPCR stop assay of DNA from CEM cells incubated with HMAF for 4 hr

Drug	Concentration (μM)	β-Globin (relative amplification)	HPRT (relative amplification)
Control		1	1
Cisplatin	200	0.1 ± 0.04 (N = 2)*	0.01 ± 0.01 (N = 2)
Adozelesin	0.1	ND†	0.17 ± 0.1 (N = 2)
HMAF	25	0.68 ± 0.09 (N = 4)	1.01 ± 0.4 (N = 5)
	50	0.99 (N = 1)	0.99 ± 0.04 (N = 2)
	100	0.84 ± 0.06 (N = 4)	1.30 ± 0.15 (N = 5)
	200	0.68 (N = 1)	1.21 ± 0.05 (N = 2)

Data show the relative amplification (± SEM). N = number of independent determinations.
* Where N = 2, values are averages ± one-half of the range.
†ND = not determined.

evaluated by electron microscopy under 2000× original magnification.

Precursor Incorporation

CEM cells (5×10^5 cells/mL) were incubated with HMAF for 4 hr at 37°, followed by a 30-min incubation with a ^{3}H-labeled precursor (thymidine, uridine, or leucine) at 2 μCi/mL. Cells for leucine incorporation were suspended in leucine-free medium for the duration of the experiment. Sample processing to detect radioactivity incorporated into macromolecules (PCA-insoluble) was carried out as described previously [23, 24]. The results are expressed as a percentage of precursor incorporation into untreated cells.

Ribonucleotide Levels in HMAF-Treated CEM Cells

A standard HPLC procedure was used to analyze the intracellular ribonucleotide pools [25]. PCA-extracted nucleosides and nucleotides (mono-, di- and triphosphates) were separated in a linear gradient of potassium phosphate buffer, pH 4.5 (10–500 mM), on a Partisil 10 SAX column (Whatman) using a computer-controlled Beckman gradient HPLC system. Nucleotide peaks were identified based on retention times of appropriate standards.

RESULTS

HMAF Cytotoxicity Against CEM Cells

Previous studies with other illudins showed a broad range of cytotoxic activities depending on the cell line [2]. HMAF showed significant cytotoxic activity against human leukemia CEM cells (EC_{50} = 1.7 ± 0.2 μM) following a 72-hr continuous incubation under the standard conditions of our MTT assay. Thus, CEM leukemia is a cell line that is sensitive to HMAF [10].

Modest Effect of HMAF Treatment on DNA Template Properties

Various DNA lesions impede DNA template properties, reducing the amplification of a damaged template in PCR reactions [14]. Therefore, the efficiency of amplification of DNA from drug-treated cells, monitored by the QPCR Stop Assay, provides an overall measure of DNA damage. We examined the ability of HMAF to affect DNA amplification by using the QPCR Stop Assay for a segment of the β-globin gene and another region at the hypoxanthine phosphoribosyltransferase (HPRT) locus (Table 1). HMAF at 25–200 μM produced a partial inhibition of the β-globin gene amplification with no clear dependence on drug level. Examination of the same DNA preparations for their ability to amplify the HPRT locus indicated a negligible effect of HMAF. In contrast, other alkylating drugs used as positive controls (i.e. cisplatin, a G-alkylating agent [26], and adozelesin, an AT-alkylating agent [27]) produced a potent inhibition of amplification. Thus, either HMAF-induced lesions can be readily bypassed by *Taq* polymerase or their levels are relatively low.

Lack of Bifunctional Lesions in Cellular DNA

Illudin S and related compounds have been postulated to form covalent adducts with DNA [5, 12], suggesting the possibility that HMAF could induce bifunctional lesions in genomic DNA [11]. Since bifunctional lesions are, in general, more cytotoxic than monoadducts, we analyzed the ability of HMAF to form DPC and interstrand DNA cross-links in CEM cells.

The results for DPC determinations are shown in Table 2. Incubation of CEM cells with positive control drugs (formaldehyde, nitracrine, and cisplatin) resulted in a significant fraction of total cellular DNA co-precipitating with cellular proteins. In contrast, HMAF (1–50 μM) did not induce significant DPC above background levels. These results indicate that in intact cells, HMAF does not form detectable cross-links between DNA and proteins. The formation of DPC by HMAF was marginal, even in isolated nuclei in the absence of uptake limitations and possible trapping of the drug by serum proteins and/or cytoplasmic thiols (data not shown).

The potential of HMAF to induce another type of bifunctional lesion, interstrand DNA cross-links, was examined by alkaline sucrose sedimentation. DNA from

TABLE 2. DPC in CEM cells measured by K^+/SDS precipitation

Drug	Concentration (μM)	DPC (% total DNA)
Control		1.8 ± 0.2
Formaldehyde	1000	73.3 ± 1.9
Nitracrine	20	16.7 ± 1.2
Cisplatin	50	15.4 ± 1.1
HMAF	1	1.9 ± 0.1
	5	2.2 ± 0.1
	10	2.5 ± 0.2
	50	2.6 ± 0.2

Incubation with HMAF was for 4 hr. The results show the fraction of total DNA co-precipitating with proteins (average values from two independent determinations ± one-half of the range). Formaldehyde, nitracrine, and cisplatin were used as positive controls.

untreated cells sedimented to the middle of the gradients under conditions optimized for interstrand DNA cross-link detection (Fig. 2A). Cross-linking, for instance by cisplatin, prevents alkali-induced strand separation so cross-linked DNA sediments at a higher apparent molecular weight, resulting in a sedimentation profile shifted toward the bottom of the gradients [28] (also data not shown). HMAF treatment did not result in such downward shifts. In contrast, slight shifts of DNA profiles toward the top of the gradients (i.e. toward smaller DNA sizes) were noted. Thus, HMAF does not induce a significant amount of interstrand DNA cross-links under these conditions.

Induction of Single-Strand Breaks by HMAF in Cellular DNA

A gradual shift toward smaller DNA sizes, as seen in Fig. 2A, if verified, might indicate drug-induced strand scissions. Such an effect might reflect an inherent strand scission ability of HMAF. Alternatively, strand breakage could be a secondary consequence of drug action, such as breaks generated in the course of DNA repair or in the early stages of apoptosis. To verify the induction of strand breaks and distinguish among these possibilities, we employed sedimentation conditions optimized for strand-break detection (Fig. 2, B and C). Under these conditions, DNA from untreated cells sedimented to the bottom half of the gradients as a broad band. The sedimentation profiles for cells treated with HMAF at 10 or 50 μM indicated smaller DNA fragments with a maximum corresponding to ~80 kb (fractions 12–13).

Interestingly, DNA breaks, induced by a short treatment with HMAF, were not readily reversible. Instead, the magnitude of strand breakage increased markedly during a post-treatment incubation (Fig. 2C). Fragments as small as 2–4 kb appeared on the gradients (fractions 3–4, Fig. 2C).

Lesions detected by alkaline sedimentation may reflect not only true single-strand breaks but also alkali-labile sites. To obtain an independent measure of true single-strand breaks, we employed nucleoid sedimentation analysis [17].

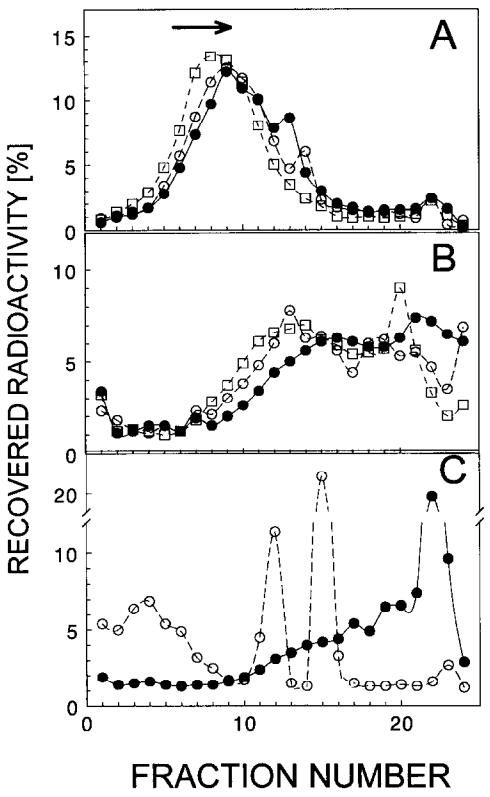

FIG. 2. Effects of HMAF at 0 μM (●), 10 μM (○), and 50 μM (□) on the sedimentation of DNA from CEM cells on alkaline sucrose gradients. (A) Lack of interstrand cross-links in CEM cells treated with HMAF for 4 hr at 37° (sedimentation conditions optimized for the detection of DNA interstrand cross-links). (B) DNA-strand breakage in cells treated with HMAF for 4 hr and analyzed immediately (sedimentation conditions optimized for the detection of strand breaks). (C) Same as panel B but following post-incubation in drug-free medium for an additional 17 hr. The profile for 50 μM HMAF (omitted for clarity from panel C) showed extensive fragmentation similar to the profile for 10 μM drug. In panels B and C, the material near the bottom of the gradient (fraction 22, maximum for control DNA) corresponds to ~150 S or ~1300 kb DNA. Fractions 12, 9, and 4 correspond to ~80, ~40, and ~4 kb, respectively. The arrow in panel A indicates the direction of sedimentation.

Nucleoids are residual nuclear structures that survive histone removal and consist of DNA loops attached to the nuclear matrix [29]. Because of the association with the nuclear matrix, DNA loops maintain their original supercoiling. Strand scissions cause loop relaxation that can be monitored as slower nucleoid sedimentation. This assay is performed under neutral conditions and is a sensitive method for the detection of low levels of single-strand breaks.

Figure 3A shows representative sedimentation profiles that illustrate the effects of HMAF. Nucleoids from drug-treated cells sedimented slower than control nucleoids at HMAF levels as low as 2 μM, which is close to the EC_{50} value. Normalized nucleoid sedimentation for several drug concentrations (Fig. 3B) showed that the effect plateaus at ~10 μM HMAF. Such a plateau would occur when the

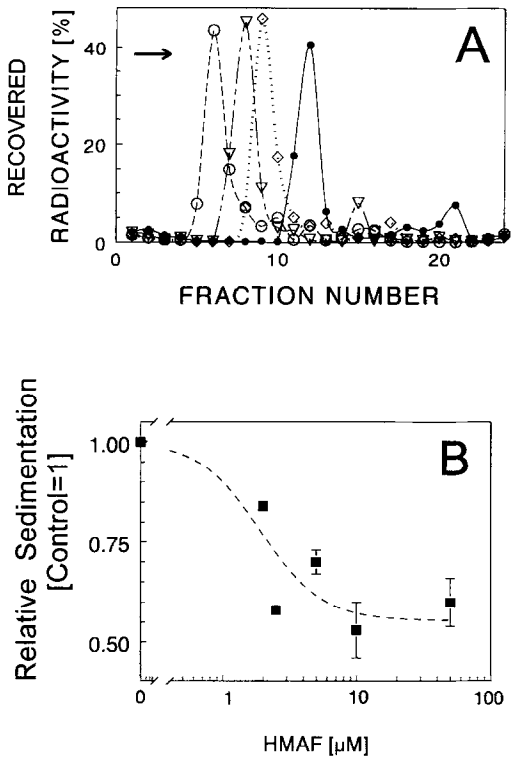

FIG. 3. Effect of HMAF on sedimentation of nucleoids from CEM cells (assay for single-strand breaks). Incubation with HMAF was for 4 hr. (A) Representative sedimentation profiles of nucleoids from cells incubated with HMAF at 0 μM (●), 2 μM (◇), 5 μM (▽), and 10 μM (○). (B) Relative sedimentation (normalized for sedimentation of nucleoids from untreated cells) from at least two experiments (averages ± one-half of the range).

DNA loops are completely relaxed (i.e. with at least one break per loop). Hence, a 4-hr incubation of CEM cells with 10 μM HMAF generated roughly one single-strand break per DNA loop, which is equivalent to 1 break per 60–90 kbp, assuming a typical loop size [29]. These estimates corroborate the findings by alkaline sedimentation and confirm that HMAF induces true strand breaks in cellular DNA.

On the other hand, HMAF was unable to relax naked supercoiled DNA (i.e. to form DNA strand breaks) in a cell-free environment even during a prolonged (24-hr) incubation (data not shown). Thus, strand breaks in cellular DNA, even after short treatments, probably result from an indirect effect rather than from inherent strand scission activity of HMAF. Moreover, the enhancement of DNA damage following drug removal suggests that HMAF-induced lesions actually reflect drug-induced apoptotic DNA degradation.

Apoptotic Fragmentation: Generation of Small Double-Stranded DNA by HMAF

A hallmark of apoptosis is endonucleolytic cleavage of nucleosomal "linker" DNA that ultimately leads to short double-stranded fragments, often but not always, down to mono-, di-, and trinucleosomal sizes [30, 31]. Such fragments can be quantitated based on their release from nuclei under hypotonic conditions [18]. Thus, we measured the formation of small DNA fragments in cells treated with HMAF for 4 hr and post-incubated in drug-free medium (i.e. under conditions that greatly enhanced HMAF-induced single-strand breaks). Figure 4A shows that HMAF induced the generation of short radiolabeled double-stranded DNA fragments in drug-treated cells. The magnitude of this effect depended on drug concentration. At high HMAF levels (50 μM), as much as 35% of total cellular DNA became fragmented. Most of the released fragments were between ~8 and 15 kbp, as estimated by agarose electrophoresis (Fig. 4B). However, even excessive fragmentation did not generate significant amounts of nucleosomal-size material ("nucleosomal ladder") as found by agarose electrophoresis (data not shown).

The presence of the protein synthesis inhibitor cycloheximide during and after the incubation with HMAF had very little effect, if any, on the release of DNA fragments (data not shown). Hence, HMAF effects do not require new protein synthesis. On the other hand, when Zn^{2+}, a potent inhibitor of endonucleases and apoptosis (reviewed by Sunderman [32]), was present, DNA fragmentation was abolished (Fig. 4A). Zinc prevention of DNA fragmentation has been interpreted by numerous other studies as the inhibition of apoptosis resulting from the inhibition of zinc-dependent nucleases [32, 33]. Hence, the results with zinc corroborate apoptosis induction by HMAF, although these data need to be interpreted with caution since $ZnSO_4$ is, itself, toxic to cells [32, 33].

HMAF Effects on Cell Cycle

We examined HMAF effects on cell cycle progression by flow cytometry under standard conditions that allowed fragmented DNA to elute from apoptotic cells when permeabilized for staining with PI. While HMAF effects depended on drug concentrations and times of incubation (Fig. 5A), a consistent outcome was the accumulation of cells in the S phase. Histogram deconvolution (as in Fig. 5B) allowed for the quantitation of these data. For example, for 17 hr of treatment (Fig. 5C), the S phase fraction amounted to ~77 and 80% cells, with 3.4 and 8.5 μM HMAF, respectively, compared with ~43% for the untreated control. This accumulation appeared to occur in an early S phase, particularly for treatment conditions resulting in profound apoptotic changes (see below).

HMAF action also resulted in the progressive generation of particles corresponding to hypodiploid DNA content (sub-G_1 material) that is characteristic of apoptosis and reflects fragmented DNA leaking from stained cells [34]. Quantitation of the sub-G_1 material is plotted along with the cell viability data (Fig. 5D). Elevated levels of sub-G_1 material were seen for each drug concentration tested. Under some conditions (e.g. after 17 hr of treatment with

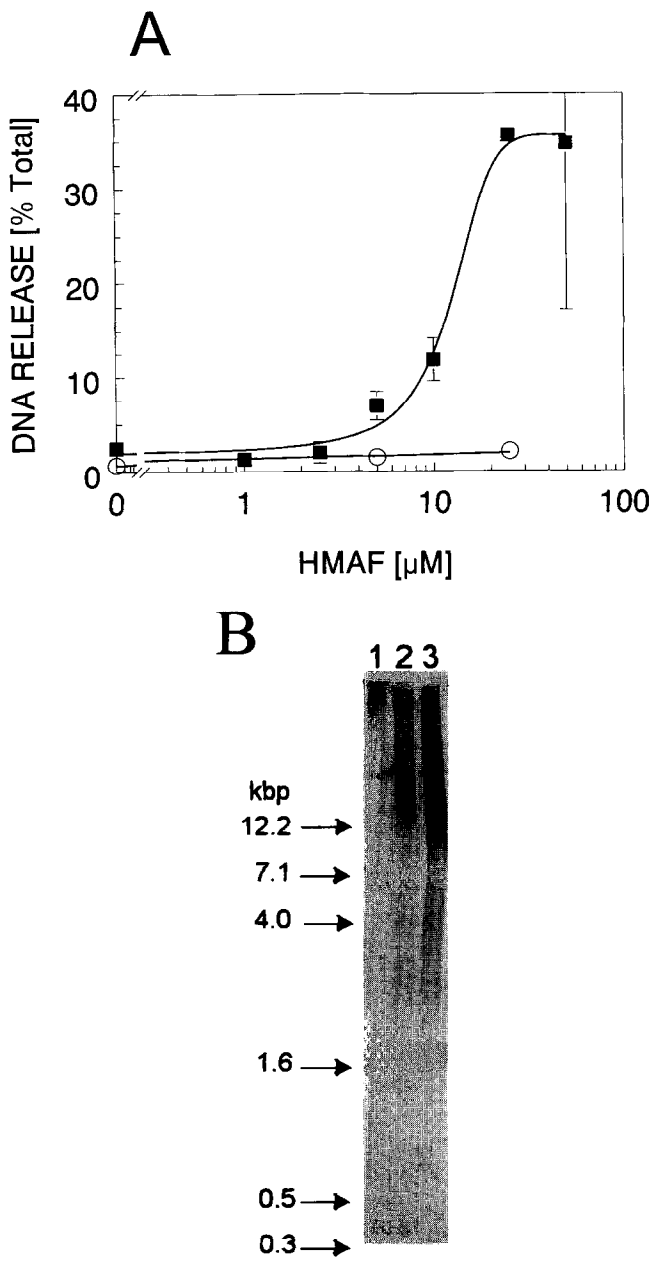

FIG. 4. HMAF-induced double-stranded DNA cleavage in CEM cells. Cells with [^{14}C]thymidine-prelabeled DNA were treated with HMAF for 4 hr and post-incubated in HMAF-free medium for an additional 17 hr. The cells were permeabilized and short double-stranded DNA fragments extracted as described in "Materials and Methods." (A) The release of DNA fragments for cells treated with HMAF only (■) and HMAF and 0.5 mM $ZnSO_4$ (○). $ZnSO_4$, when included, was present during the entire 21-hr incubation. The points represent the mean values (± SEM) from 1–4 separate experiments carried out in duplicate. (Where N = 2, values are averages ± one-half of the range.) Under these conditions, Adriamycin® at 0.5 μM released 47.1 ± 9.3% DNA. For 50 μM HMAF, some radioactivity (~5% total) was found in culture medium and PBS wash. Such a release was insignificant for lower drug levels (data not shown). (B) Autoradiogram of the electrophoresis (in 0.8% agarose) of the released fragments from cells treated with HMAF at 0 μM (lane 1), 5 μM (lane 2), and 25 μM (lane 3). DNA sizes are based on markers visualized by ethidium bromide.

8.5 μM HMAF), the sub-G_1 material formed a distinct peak (Fig. 5B). Longer times of drug treatment were needed to induce the sub-G_1 material for lower drug levels (Fig. 5, A and D). Such a pattern—extensive debris formation and a distinct "apoptotic" peak—has been observed for other drugs that induce apoptosis and generate apoptotic bodies [34].

The appearance of the sub-G_1 material in the flow cytometry histograms at cell growth inhibitory concentrations of HMAF seemed to precede significant changes in cell viability (Fig. 5D). For instance, HMAF at 1.7 μM (1 × EC_{50}) produced a minimal effect on cell viability for up to 48 hr while inducing a significant amount of the sub-G_1 material and inhibition of cell growth. A precedence of sub-G_1 induction over viability reduction was less pronounced but still noticeable after 72 hr at 1.7 μM HMAF and after 24 and 48 hr for 3.4 μM HMAF. This pattern is consistent with the notion that cells in the early stages of apoptosis have intact cell membranes. A plausible explanation for HMAF membrane effects at higher drug levels and/or very long treatments is that cells in the advanced stages of apoptosis may lose membrane integrity due to secondary necrosis [35].

HMAF Induction of Apoptotic Morphological Changes

The interpretation of "apoptotic" assays that measure DNA fragmentation is uncertain unless characteristic morphological changes are also present. To verify that CEM cells initiate apoptosis following HMAF treatment, we analyzed cell morphology by electron microscopy. The ultrastructural features of apoptosis include chromatin condensation, compactness of cytoplasmic organelles, and the appearance of protuberances on the cell surface [36, 37]. Untreated CEM cells (Fig. 6A) had recognizable cytoplasm, scattered microvilli features on the plasma membrane, and a convoluted nucleus with dispersed chromatin. HMAF-treated cultures included cells showing typical apoptotic features (Fig. 6B). Cells containing compacted, electron-dense chromatin were observed, sometimes clearly demarcated from the decondensed chromatin in a nucleus, forming a crescent-shaped density along the edge of a micronucleolus. The cells displaying chromatin condensation still had intact plasma membranes with recognizable cytoplasmic organelles.

HMAF-Induced Apoptotic Changes by Multiparametric Flow Cytometry

To further characterize HMAF-induced apoptosis, we used multiparametric cytofluorimetric analysis. In these experiments, apoptotic cells were detected based on tagging the 3′-OH termini at DNA cleavage sites with biotin-labeled deoxynucleotides using exogenous TdT. At the same time, DNA content was measured to determine cell cycle progression. Forward- and side (orthogonal)-light scattering were used to assess the effects of HMAF on cell optical properties that can be indicative of changes in cell size, cell

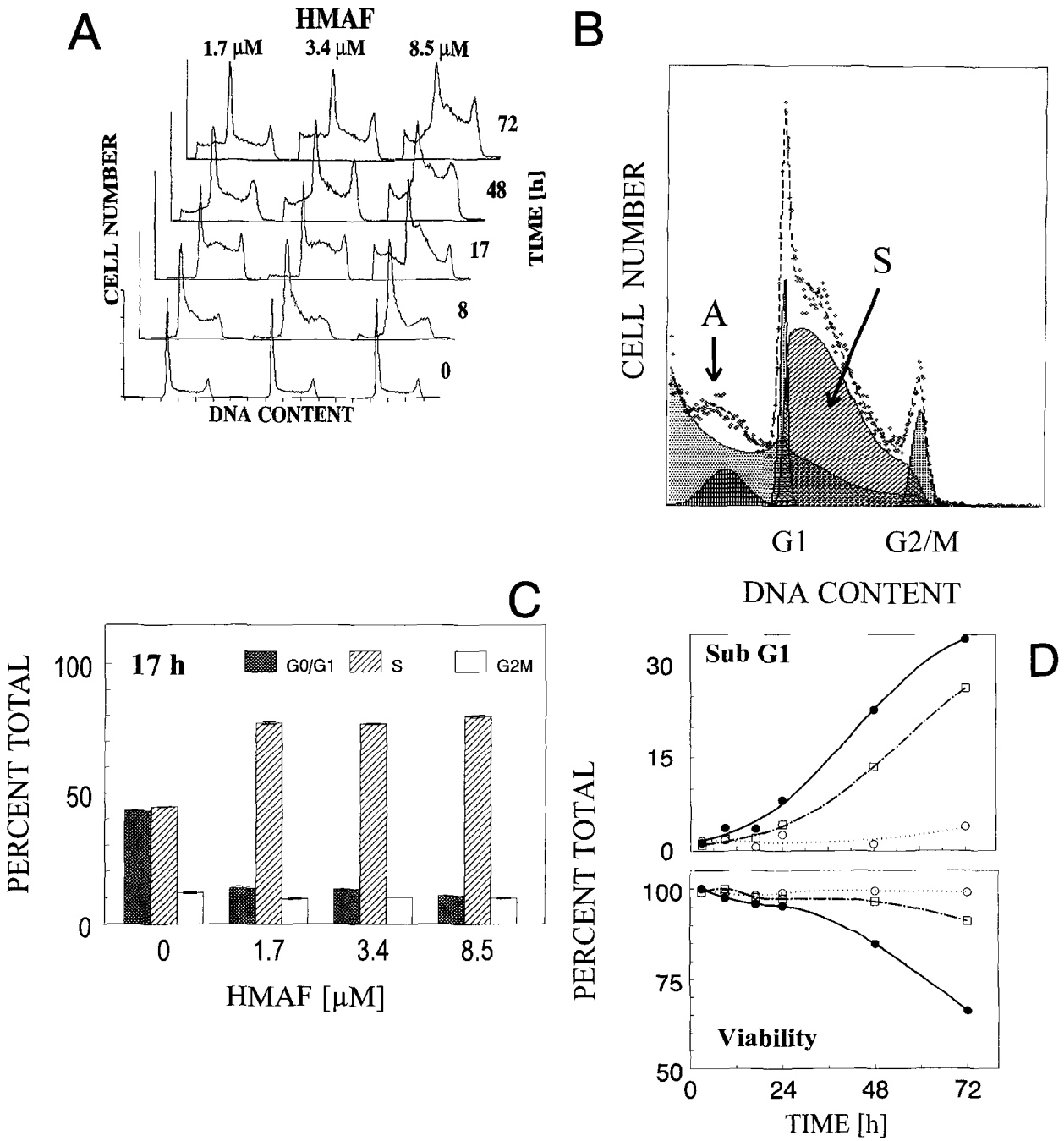

FIG. 5. HMAF effects on cell cycle traverse in CEM cells by flow cytometry (PI staining). (A) Representative histograms for cells incubated with various concentrations of HMAF for indicated times. Histograms for control cells after various incubation times (not shown) did not differ markedly from those shown for 0-hr treatments with HMAF. (B) Flow cytometry histogram for cells treated with 8.5 μM HMAF for 17 hr showing sub-G_1 material, indicative of apoptotic cells. Note a distinct apoptotic peak (marked with an "A"). To quantitate flow cytometry data, the histograms were deconvoluted to get sub-G_1 and individual cell cycle compartments as illustrated in this example. For the conditions shown, the sub-G_1 material amounted to 15.5 ± 7.45% of total events scored (± one-half of the range). (C) The proportion of cells in various phases of the cell cycle after a 17-hr treatment with HMAF (± one-half of the range). (D) The quantitation of sub-G_1 events (top) and cell viability (by trypan blue exclusion, bottom) after various times of incubation with HMAF at 0 μM (○), 1.7 μM (□), and 3.4 μM (●). Data from two experiments are pooled together.

surface, and other morphological characteristics (Fig. 7). Unlike the data in Fig. 5, the leakage of fragmented chromatin from nuclei was prevented in these determinations by using paraformaldehyde fixation.

Figure 7A shows examples of the bivariate histograms showing cells with fragmented DNA (positive for TdT-mediated staining) as a function of DNA content (PI staining), forward scatter, and side scatter. Incubation with HMAF profoundly increased the number of cells capable of TdT staining. Most of these cells had G_1 or early S DNA

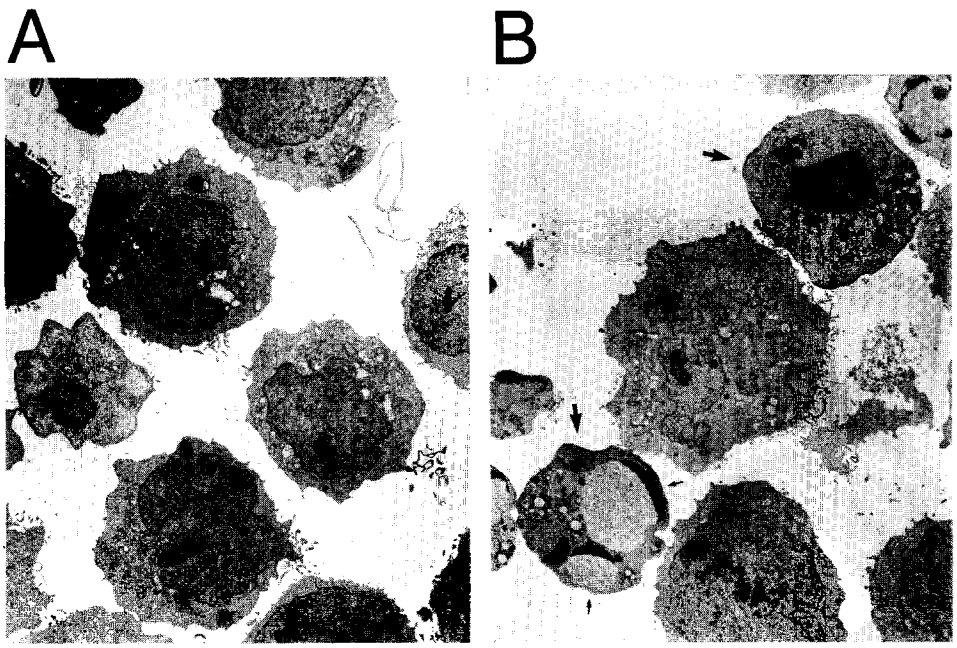

FIG. 6. Apoptotic morphological changes induced by HMAF in CEM cells. Electron microscopy of CEM cells treated for 20 hr with HMAF at 0 μM (A) and 3.4 μM (B). Large and small arrows indicate cells with condensed chromatin, with small arrows marking crescent shape electron dense areas along the margins of micronucleoli. Representative fields from duplicate samples are shown. The original magnification was 2000×.

content, suggesting that cells in these phases of the cell cycle are most susceptible to apoptosis induction by HMAF. Forward scatter and side scatter data indicate dramatic morphological changes in HMAF-treated CEM cells. The subpopulations of cells detected by both types of light scattering coincided to a large extent with the apoptotic cells found, based on DNA fragmentation versus DNA content plots.

The fraction of cells with apoptotic DNA fragmentation, as assessed by the TdT assay, showed a clear dependence on the time of treatment (Fig. 7B). Significant apoptotic strand breaks could be seen with HMAF at 3.4 μM (2 × EC_{50}) after a 17-hr incubation but not after a 4-hr treatment. This effect was preceded by an increase in the proportion of cells in S phase (detectable already at 1.7 μM HMAF). Interestingly, the assessment based on light-scattering data shows approximately 50% more of presumably apoptotic cells. Hence, the TdT assay might not detect less frequent apoptotic cleavages in cells that already exhibit apoptotic morphological changes (such as shrinkage) that affect their light-scattering properties. Given the absence of DNA degradation to mononucleosomal fragments in HMAF-treated cultures (shown in the previous assays), it is likely that morphological changes may precede TdT-detectable DNA fragmentation.

Preferential Inhibition of DNA Synthesis by HMAF

The ability of HMAF to block cells in the S phase suggests that the drug may inhibit DNA replication. In fact, HMAF was a potent inhibitor of DNA synthesis with IC_{50} = 2 μM as found based on [^{3}H]thymidine incorporation (data not shown). The inhibition of RNA synthesis was observed at higher drug levels with IC_{50} = 20 μM. In contrast to nucleic acid synthesis, protein synthesis was somewhat stimulated at lower drug levels and inhibited only at very high HMAF concentrations (IC_{50} = 70 μM).

Inhibition of thymidine or uridine incorporation does not seem to reflect an effect on *de novo* precursor synthesis. Ribonucleotide levels in extracts from cells treated with HMAF for up to 24 hr showed no dramatic changes, although the levels of most ribonucleotides were elevated slightly compared with untreated controls (Table 3 and data not shown). Such an elevation of ribonucleotide pools could be explained by a feedback inhibition of ribonucleotide conversion to deoxyribonucleotides resulting from the inhibition of DNA synthesis. In addition, slightly elevated levels of ATP demonstrated that HMAF does not affect energy-generating processes.

DISCUSSION

The mechanism by which HMAF, a new promising drug in clinical trials, inhibits cell growth remains largely unstudied. This investigation is one of the first mechanistic characterizations of this drug. Our results show that HMAF affects the integrity of genomic DNA. Whereas HMAF has a potential to alkylate cellular nucleophiles, the lesions observed in genomic DNA reflect predominantly secondary damage, probably apoptotic DNA strand breakage. The induction of apoptotic strand breaks parallels a preferential inhibition of DNA synthesis, a block in S phase of the cell cycle, and, finally, cell growth inhibition. The observed pattern is consistent with apoptosis being involved in the antiproliferative effects of HMAF. To our knowledge, HMAF is the only illudin for which apoptosis induction has been demonstrated.

The effects of HMAF on cellular DNA are somewhat surprising. Under the conditions of our assays, neither interstrand DNA cross-links nor DNA–protein cross-links

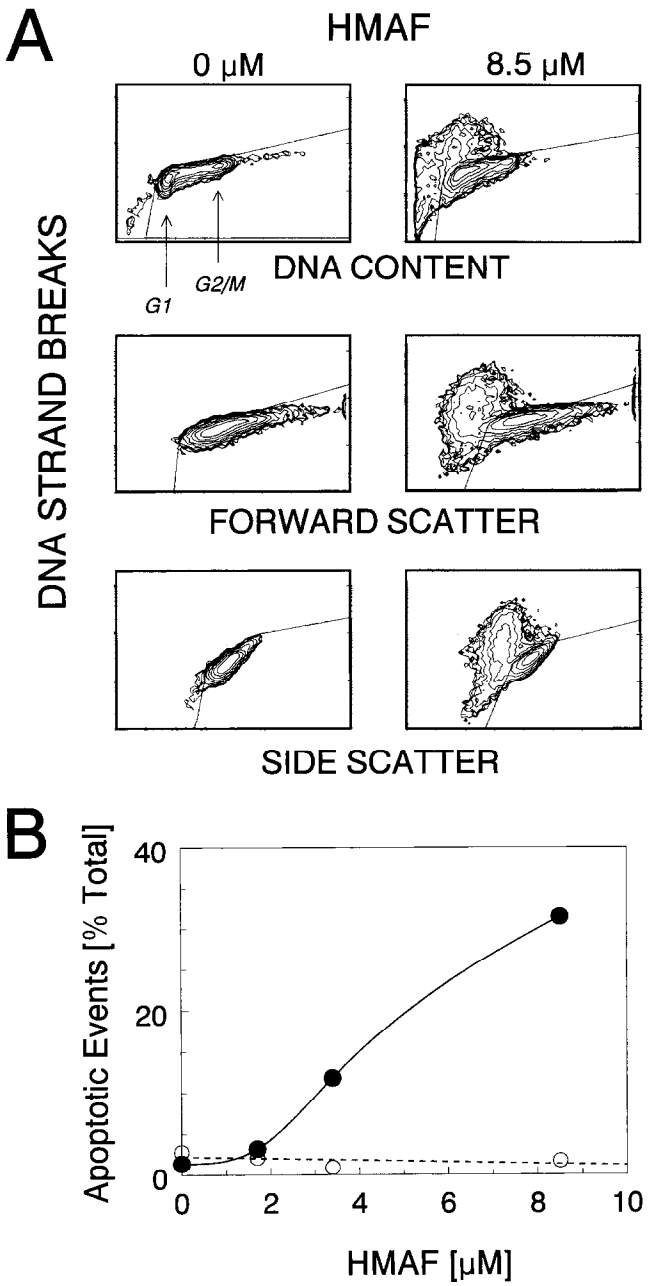

FIG. 7. Multiparametric flow cytometry analysis of HMAF-treated CEM cells. (A) Sample bivariate histograms are shown for control cells and cells treated with 8.5 μM HMAF for 21 hr. Apoptotic strand breakage data (by TdT) are plotted against DNA content (by PI), forward scatter, and side scatter. (B) Quantitation of apoptotic cells (population with elevated apoptotic breaks based on TdT assay) in cultures incubated with HMAF for 4 hr (○) and 21 hr (●). Typical variability for replicate cultures did not exceed 1 to 1.5%.

were detected in cellular DNA. Thus, the suggestion that certain illudins may form bifunctional adducts with nucleophiles including DNA [3] may not pertain to HMAF. HMAF also had little effect on the ability of DNA from drug-treated cells to serve as a template in primer extension. However, the drug is still likely to form monoadducts to cellular DNA. Our recent determinations confirmed the ability of ^{14}C-labeled HMAF to bind to DNA, although proteins appeared to be more extensively adducted (Herzig M and Woynarowski JM, unpublished results).

HMAF-induced secondary DNA strand scissions were demonstrated using several methods. Both single- and double-strand breaks were detected at HMAF concentrations that are pharmacologically relevant in terms of cell growth inhibition. During the initial period of incubation, mostly large fragments (with a peak at ~80 kb) were formed. Prolonged incubation, however, resulted in profoundly shorter fragments (~2–4 kb). Moreover, HMAF effects, once initiated, were not readily repairable and progressed further to short fragments during a prolonged incubation, even in the absence of the drug.

The observed breakage of cellular DNA by HMAF shows the characteristics of apoptotic DNA fragmentation [30, 31, 38]. During apoptosis, DNA fragmentation progresses through a temporally ordered series of stages [30, 31] commencing with the production of DNA fragments of ~50 to ~300 kbp, which are further degraded, typically over several hours, to smaller fragments [30, 31, 34]. As with the HMAF effects, such a progression continues even following the removal of the apoptosis inducer. DNA fragments generated by apoptosis feature 3′-OH groups [21, 22], as confirmed for HMAF by the TdT assay. Also, prevention of HMAF-induced DNA fragmentation by $ZnSO_4$, but not by cycloheximide, is consistent with the findings for other apoptotic stimuli [33, 39]. What is less typical in HMAF-induced apoptosis is that the fragments generated were larger than the "classical" nucleosomal ladder. However, oligonucleosomal fragmentation, although often characteristic, may not be a critical event for apoptotic death, and apoptosis in the absence of the nucleosomal ladder has been observed by others [40–43].

While the extensive DNA fragmentation observed after prolonged treatment with HMAF was clearly apoptotic, the early breakage of cellular DNA might conceivably reflect direct strand scissions. Such direct breaks might thus be an apoptotic inducer as found for other DNA-damaging agents [30, 31]. However, HMAF does not induce strand breaks in purified DNA. Unlike HMAF, typical strand scission drugs (inducing direct, non-apoptotic breaks) can generate small DNA fragments of nucleosomal or subnucleosomal length, even after a brief incubation [44]. Also, a significant proportion of such direct breaks is repaired during a post-treatment incubation [38], which is not the case with HMAF. Hence, the low levels of breaks in cellular DNA observed after brief treatments with HMAF probably reflect early stages of apoptosis.

Besides biochemical indicators of DNA fragmentation, HMAF induces morphological changes that are characteristic of apoptosis, such as chromatin condensation and cell shrinkage demonstrated by electron microscopy (Fig. 6 and data not shown). HMAF action resulted in discrete subpopulations of cells that showed anomalous light scattering, indicating altered cell morphology. Also, cells (and/or particles) with sub-G_1 DNA content were detected, which

TABLE 3. HMAF effects on ribonucleotide levels in CEM cells incubated with the drug for 24 hr

HMAF* (μM)	Nucleotides (nmol/10^7 cells)†							
	UDP	CDP	ADP	GDP	UTP	CTP	ATP	GTP
0	2.9	1.2	11.8	3.2	4.2	1.9	13.7	3.6
1	3.4	1.5	14.6	4.4	4.3	1.9	15.0	4.1
2	4.7	2.2	17.9	5.5	8.2	4.4	30.0	8.9

Intracellular pools of ribonucleotides were determined in PCA extracts from drug-treated cells, as described in Materials and Methods.

* At these concentrations, HMAF did not reduce cell viability significantly, as measured by trypan blue exclusion. Results for drug levels > 2 μM were omitted since they might have been affected by the possible leakage of ribonucleotides from cytoplasm.

†Typical variability of nucleotide levels in replicate cultures did not exceed 5–15%.

is another indicator of apoptosis [34, 45]. These cytofluorimetric characteristics showed a very similar time and concentration dependence to TdT analysis and biochemical assays of DNA fragmentation.

HMAF increases the proportion of cells in the S phase, with cell accumulation close to the G_1/S border accompanying a pronounced apoptosis induction. On the other hand, TdT and light-scattering analysis suggested that apoptosis occurred mainly to cells in the G_1 phase. Apoptotic death of G_1 and early S cells may be related to the HMAF-induced block of the cell cycle traverse in S phase. Preliminary experiments with synchronized cultures suggest that cells exposed to the drug in a late S phase proceed to G_1 in the next cell cycle before they undergo apoptosis, while surviving cells become blocked in S (data not shown).

Consistent with the S phase block, HMAF is a preferential inhibitor of DNA synthesis. While a slight elevation of ribonucleotide triphosphates is an expected outcome of such an inhibition, the unimpeded ATP production shows also that HMAF-induced apoptosis and cell growth inhibition are not accompanied by a general inhibition of cellular metabolism. Overall, HMAF appears to resemble Illudin S, which was also found to preferentially inhibit DNA synthesis, block cells in the G_1/S, and bind to cellular DNA [2, 12]. Interestingly, the superior pharmacological properties of HMAF were accompanied by a markedly lower cytotoxicity than that of Illudin S [2].

Apoptotic DNA degradation may be an important factor in the antiproliferative action of HMAF, in general. For example, preliminary results show a comparable level of apoptosis in COLO320DM cells (data not shown). Further studies are needed, however, to elucidate the nature of the apoptotic stimulus of HMAF. Apoptosis induction by alkylating agents that are used clinically, unlike that by HMAF, is usually related to their ability to form bifunctional lesions with cellular DNA. Other common antitumor agents may induce apoptosis by causing direct strand breaks, topoisomerase-mediated lesions, mitotic blocks, or antimetabolitic inhibition of DNA synthesis [18, 30, 31, 33, 41]. Apoptosis induction by HMAF might originate from the ability of the drug to monoalkylate DNA. As mentioned, ^{14}C-labeled HMAF formed adducts with cellular DNA, although cellular proteins were adducted to a higher level (Herzig M and Woynarowski JM, unpublished results). Thus, in the absence of bifunctional DNA lesions, alkylation of targets other than DNA also needs to be considered as one of the possible factors in the mode of action of HMAF. In particular, HMAF binding to proteins would be consistent with illudins being reactive towards thiols [11]. By analogy to several thiol-reactive cytotoxic sesquiterpene lactones [46], HMAF may inactivate important cellular proteins by binding to their sulfhydryl groups. Studies are underway to further explore cellular targets of HMAF and the nature of drug-induced apoptosis and cell growth inhibition.

The skillful technical assistance of Mr. Richard Salinas in the flow cytometry measurements is acknowledged. The authors thank also Dr. Maryanne Herzig for a critical reading of the manuscript. This study was supported, in part, by a grant from MGI PHARMA, Inc.

References

1. Kelner MJ, McMorris TC, Beck WT, Zamora JM and Taetle R, Preclinical evaluation of illudins as anticancer agents. *Cancer Res* **47:** 3186–3189, 1987.
2. Kelner M, McMorris T and Taetle R, Preclinical evaluation of illudins as anticancer agents: Basis for selective cytotoxicity. *J Natl Cancer Inst* **82:** 1562–1565, 1990.
3. McMorris TC, Kelner MJ, Chandha RK, Siegel JS, Moon S and Moya MM, Structure and reactivity of illudins. *Tetrahedron* **45:** 5433–5440, 1989.
4. Shinozawa S, Tsutsui K and Oda T, Enhancement of the antitumor effect of illudin S by including it into liposomes. *Experientia* **35:** 1102–1103, 1979.
5. Kelner MJ, McMorris TC and Taetle R, *In vitro* and *in vivo* studies on the anticancer activity of dehydroilludin M. *Anticancer Res* **15:** 873–878, 1995.
6. Kelner MJ, McMorris TC, Estes L, Starr RJ, Rutherford M, Montoya M, Samson KM and Taetle R, Efficacy of Acylfulvene Illudin analogues against a metastatic lung carcinoma MV522 xenograft nonresponsive to traditional anticancer agents: Retention of activity against various mdr phenotypes and unusual cytotoxicity against ERCC2 and ERCC3 DNA helicase-deficient cells. *Cancer Res* **55:** 4936–4940, 1995.
7. McMorris TC, Kelner MJ, Wang W, Yu J, Estes LA and Taetle R, (Hydroxymethyl)acylfulvene: An illudin derivative with superior antitumor properties. *J Nat Prod* **59:** 896–899, 1996.
8. McMorris TC, Hu Y, Yu J and Kelner MJ, Total synthesis of hydroxymethylacylfulvene, an antitumour derivative of illudin S. *J Chem Soc Chem Commun* **3:** 315–316, 1997.
9. Kelner MJ, McMorris TC, Estes L, Wang W, Samson KM and Taetle R, Efficacy of HMAF (MGI-114) in the MV522 metastatic lung carcinoma xenograft model nonresponsive to

traditional anticancer agents. *Invest New Drugs* **14:** 161–167, 1996.
10. MacDonald JR, Muscoplat CC, Dexter DL, Mangold GL, Chen SF, Kelner MJ, McMorris TC and Von Hoff DD, Preclinical antitumor activity of 6-hydroxymethylacylfulvene, a semisynthetic derivative of the mushroom toxin illudin S. *Cancer Res* **57:** 279–283, 1997.
11. McMorris TC, Kelner MJ, Wang W, Moon S and Taetle R, On the mechanism of toxicity of illudins: The role of glutathione. *Chem Res Toxicol* **3:** 574–579, 1990.
12. Kelner MJ, McMorris TC, Estes L, Rutherford M, Montoya M, Goldstein J, Samson K, Starr R and Taetle R, Characterization of illudin S sensitivity in DNA repair-deficient Chinese hamster cells. Unusually high sensitivity of ERCC2 and ERCC3 DNA helicase-deficient mutants in comparison to other chemotherapeutic agents. *Biochem Pharmacol* **48:** 403–409, 1994.
13. Chen SF, Behrens DL, Behrens CH, Czerniak PM, Dexter DL, Dusak BL, Fredericks JR, Gale KC, Gross JL, Jiang JB, Kirschenbaum MR, McRipley RJ, Papp LM, Patten AD, Perrella FW, Seitz SP, Stafford MP, Sun JH, Sun T, Wuonola MA and Von Hoff DD, XB596, a promising bis-naphthalimide anti-cancer agent. *Anticancer Drugs* **4:** 447–457, 1993.
14. Daoud SS, Clements MK and Small CL, Polymerase chain reaction analysis of cisplatin-induced mitochondrial DNA damage in human ovarian carcinoma cells. *Anticancer Drugs* **6:** 405–412, 1995.
15. Woynarowski JM, McNamee H, Szmigiero L, Beerman TA and Konopa J, Induction of DNA–protein crosslinks by antitumor 1-nitro-9-aminoacridines in L1210 leukemia cells. *Biochem Pharmacol* **38:** 4095–4101, 1989.
16. Woynarowski JM, McHugh MM, Gawron LS and Beerman TA, Effects of bizelesin (U-77779), a bifunctional alkylating minor groove binder, on genomic and simian virus 40 DNA. Specific damage to AT rich regions. *Biochemistry* **34:** 13042–13050, 1995.
17. Woynarowski JM, McCarthy K, Reynolds B, Beerman TA and Denny WA, Topoisomerase II mediated DNA lesions induced by acridine-4-carboxamide and 2-(4-pyridyl)quinoline-8-carboxamide. *Anticancer Drug Des* **9:** 9–24, 1994.
18. Ling YH, Priebe W and Perez-Soler R, Apoptosis induced by anthracycline antibiotics in P388 parent and multidrug-resistant cells. *Cancer Res* **53:** 1845–1852, 1993.
19. Skladanowski A and Konopa J, Adriamycin and daunomycin induce programmed cell death (apoptosis) in tumour cells. *Biochem Pharmacol* **46:** 375–382, 1993.
20. Jarvis WD, Turner AJ, Povirk LF, Traylor RS and Grant S, Induction of apoptotic DNA fragmentation and cell death in HL-60 human promyelocytic leukemia cells by pharmacological inhibitors of protein kinase C. *Cancer Res* **54:** 1707–1714, 1994.
21. Gorczyca W, Gong J and Darzynkiewicz Z, Detection of DNA strand breaks in individual apoptotic cells by the *in situ* terminal deoxynucleotidyl transferase and nick translation assays. *Cancer Res* **53:** 1945–1951, 1993.
22. Li X, Traganos F, Melamed MR and Darzynkiewicz Z, Single-step procedure for labeling DNA strand breaks with fluorescein- or BODIPY-conjugated deoxynucleotides: Detection of apoptosis and bromodeoxyuridine incorporation. *Cytometry* **20:** 172–180, 1995.
23. Woynarowski JM and Konopa J, Inhibition of DNA biosynthesis in HeLa cells by cytotoxic and antitumor sesquiterpene lactones. *Mol Pharmacol* **19:** 97–102, 1981.
24. McHugh MM, Woynarowski JM, Gawron LS, Otani T and Beerman TA, Effects of the DNA-damaging enediyne C-1027 on intracellular SV40 and genomic DNA in green monkey kidney BSC-1 cells. *Biochemistry* **34:** 1805–1814, 1995.
25. Chen SF, Ruben RL and Dexter DL, Mechanism of action of the novel anticancer agent 6-fluoro-2-(2′-fluoro-1,1′-biphenyl-4-yl)-3-methyl-4-quinoline carboxylic acid. *Cancer Res* **46:** 5014–5019, 1986.
26. Takahara PM, Rosenzweig AC, Frederick CA and Lippard SJ, Crystal structure of double-stranded DNA containing the major adduct of the anticancer drug cisplatin [see comments]. *Nature* **377:** 649–652, 1995.
27. Lee CS, Pfeifer GP and Gibson NW, Mapping of DNA alkylation sites induced by adozelesin and bizelesin in human cells by ligation-mediated polymerase chain reaction. *Biochemistry* **33:** 6024–6030, 1994.
28. Roberts JJ and Friedlos F, The frequency of interstrand cross-links in DNA following reaction of *cis*-diamminechloroplatinum(II) with cells in culture or DNA *in vitro*: Stability of DNA crosslinks and their repair. *Chem Biol Interact* **39:** 181–189, 1982.
29. Cook PR, The nucleoskeleton and the topology of replication. *Cell* **66:** 627–635, 1991.
30. Hickman JA, Potten CS, Merritt AJ and Fisher TC, Apoptosis and cancer chemotherapy. *Philos Trans R Soc Lond B Biol Sci* **345:** 319–325, 1994.
31. Kerr JF, Winterford CM and Harmon BV, Apoptosis. Its significance in cancer and cancer therapy [published erratum appears in *Cancer* **73:** 3108, 1994]. *Cancer* **73:** 2013–2026, 1994.
32. Sunderman FW Jr, The influence of zinc on apoptosis. *Ann Clin Lab Sci* **25:** 134–142, 1995.
33. Takano Y, Okudaira M and Harmon BV, Apoptosis induced by microtubule disrupting drugs in cultured human lymphoma cells. Inhibitory effects of phorbol ester and zinc sulphate. *Pathol Res Prac* **189:** 197–203, 1993.
34. Darzynkiewicz Z, Bruno S, Del Bino G, Gorczyca W, Hotz MA, Lassota P and Traganos F, Features of apoptotic cells measured by flow cytometry. *Cytometry* **13:** 795–808, 1992.
35. Cejna M, Fritsch G, Printz D, Schulte-Hermann R and Bursch W, Kinetics of apoptosis and secondary necrosis in cultured rat thymocytes and S.49 mouse lymphoma and CEM human leukemia cells. *Biochem Cell Biol* **72:** 677–685, 1994.
36. Wyllie AH, Morris RG, Smith AL and Dunlop D, Chromatin cleavage in apoptosis: Association with condensed chromatin morphology and dependence on macromolecular synthesis. *J Pathol* **142:** 67–77, 1984.
37. Kerr JFR, Searle J and Bishop CJ, Apoptosis. In: *Perspectives on Mammalian Cell Death* (Ed. Potten CS), pp. 93–128. Oxford University Press, Oxford, 1987.
38. Marks DI and Fox RM, DNA damage, poly (ADP-ribosyl)ation and apoptotic cell death as a potential common pathway of cytotoxic drug action. *Biochem Pharmacol* **42:** 1859–1867, 1991.
39. Gong J, Li X and Darzynkiewicz Z, Different patterns of apoptosis of HL-60 cells induced by cycloheximide and camptothecin. *J Cell Physiol* **157:** 263–270, 1993.
40. Barbieri D, Troiano L, Grassilli E, Agnesini C, Cristofalo EA, Monti D, Capri M, Cossarizza A and Franceschi C, Inhibition of apoptosis by zinc: A reappraisal. *Biochem Biophys Res Commun* **187:** 1256–1261, 1992.
41. Solary E, Bertrand R and Pommier Y, Apoptosis induced by DNA topoisomerase I and II inhibitors in human leukemic HL-60 cells. *Leuk Lymphoma* **15:** 21–32, 1994.
42. Oberhammer F, Wilson JW, Dive C, Morris ID, Hickman JA, Wakeling AE, Walker PR and Sikorska M, Apoptotic death in epithelial cells: Cleavage of DNA to 300 and/or 50 kb fragments prior to or in the absence of internucleosomal fragmentation. *EMBO J* **12:** 3679–3684, 1993.
43. Finiels F, Robert JJ, Samolyk ML, Privat A, Mallet J and Revah F, Induction of neuronal apoptosis by excitotoxins associated with long-lasting increase of 12-O-tetradecanoyl-

phorbol 13-acetate-responsive element-binding activity. *J Neurochem* **65:** 1027–1034, 1995.
44. Woynarowski JM, Gawron LS and Beerman TA, Bleomycin-induced aggregation of presolubilized and nuclear chromatin from L1210 cells. *Biochim Biophys Acta* **910:** 149–156, 1987.
45. Pelliciari C, Manfredi AA, Bottone MG, Schaack V and Barni S, A single-step staining procedure for the detection and sorting of unfixed apoptotic thymocytes. *Eur J Histochem* **37:** 381–390, 1993.
46. Grippo AA, Hall IH, Kiyokawa H, Muraoka O, Shen YC and Lee KH, The cytotoxicity of helenalin, its mono and difunctional esters, and related sesquiterpene lactones in murine and human tumor cells. *Drug Des Discov* **8:** 191–206, 1992.